Published in : Engineering (2025), vol. 337, pp. 1–14
DOI: 10. 1016/j.engstruct.2025.120502
Status : Postprint (Author's version)

Experimental investigations on the fatigue resistance of thin-walled cold-formed Z-sections

Maxime Vermeylen [a], Marios-Zois Bezas [a], Koenraad Ginckels [b], Hélène Morch [c], Jean-François Demonceau [a]

[a] *Steel and Composite Construction, UEE Research Unit, Liège University, Belgium*
[b] *Stow International, Belgium*
[c] *GDTech, Belgium*

Keywords :
Fatigue, Cold-formed sections, Thin-walled member, EN1993-1–9, Rack structures Z-section, PrEN1993-1–9

Abstract

Cold-formed thin-walled steel members are extensively used in rack storage structures due to their advantageous geometrical and mechanical properties as well as their lightweight. In multi-deep rack systems, shuttles are usually used to bring pallets to their designated storage position by rolling over elements made of Z sections. Although fatigue problems could occur on these members due to the repeated multiple passages of the shuttles, this aspect is not fully covered by EN1993–1–9, the European normative document dedicated to the fatigue design of steel structures. This paper presents and discusses the outcomes of a large experimental fatigue test campaign, in which 34 members made of thin-walled cold-formed steel Z sections were tested, in order to characterise the fatigue resistance of two specific details as part of the member. The main objective of these tests was to derive the S-N curves associated to both studied details, in accordance with the recommendations of prEN1993–1–9; these curves could finally be used by the practitioners in their design process

1. Introduction

In the face of intensifying competition in the self-supporting storage rack structures market, enhancing structural solutions and maximising the storage capacity of pallets within a given area is a key strategy for optimisation. The use of elements made of cold-formed sections could fulfil these requirements, especially in multi-deep systems configuration where multiple pallets are stocked over the same span. This system generally involves the use of an automatic shuttle that circulates on elements which carry

Published in : Engineering (2025), vol. 337, pp. 1–14
DOI: 10. 1016/j.engstruct.2025.120502
Status : Postprint (Author's version)

the pallets, and, due to the repeated journeys, they are subjected to several stress variations within a limited time. Consequently, a fatigue failure may be observed after a substantial number of load cycles.

Fatigue phenomenon has been extensively studied, with a particular emphasis on the characterisation of the fatigue resistance of structural details not yet covered by the relevant code, EN1993–1–9 [1]. Although this normative document provides design rules for structural details against fatigue, only a limited list of details is proposed in its current version, such as elements with welded parts, orthotropic desks and beams that act as a runway support. Even if the forthcoming version, prEN1993–1–9 [2], extends the number of characterised details and proposed new modified S-N curves, some elements that can be encountered in steel buildings need to be further investigated. Furthermore, the extension of the application range of these recommendations to cold-formed steel elements could be questionable, as it is not explicitly mentioned in the code. The code indicates also different methods to ensure the fatigue resistance of a given detail, such as the verification method based on damage accumulation using the S-N curve, also known as the Wholer curve. With regard to the fatigue behaviour of structural details made of cold-formed steel members for racking structures the reference normative document EN15512 [3] does not provide any recommendations.

Nevertheless, fatigue problem has been deeply studied in the recent years; most of the research focuses on the fatigue of bridges or on the behaviour of welds subjected to cyclic actions. Majeed et al. [4] present two mean stress approaches to evaluate the accumulated damage in steel bridges and propose an estimation of the remaining fatigue life. Skoglund et al. [5] study the potential improvement of two structural bridge

solutions regarding their fatigue life, by comparing them with existing details. Mouradian et al. [6] analyse a data base of 3446 experimental fatigue tests on butt-weld connections to assess the impact of various weld imperfections on the fatigue resistance. Additionally, several research on experimentally tested hot-rolled profiles are reported in the literature [7–11] and [12]. Finally, studies dealing with the revision of fatigue detail categories, can be found in [7], [13], [14] and [15].

The behaviour of raw materials and more specifically of high strength steels has been detailly investigated, as the benefits of using elements made of a higher steel grade have been clearly demonstrated in [16], [17] and [18]. De Jesus et al. [19] compare experimentally the fatigue behaviour between S355 and S690 steel grades and Chen et al. [20] investigate the fatigue characteristics of high strength steel and propose design recommendations, based on comparisons between structural details made of HSS and conventional steel grades. Further research about fatigue failure of elements made of high strength steel can be found in [21], [22] and [23].

Several investigations have been also conducted on cold-formed elements. Souto et al. [24] presents the results of an experimental fatigue test campaign performed on Z section members in the framework of the RFCS European FASTCOLD [25] project that took place from 2017 to 2020, involving academic and industrial partners. This project focuses on the fatigue assessment of cold-formed steel structural details that could be met in rack structures, such as the Z-rails subjected to loading on their flanges or beam-to-column connections. In this framework, analytical, numerical and experimental

Published in : Engineering (2025), vol. 337, pp. 1–14
DOI: 10. 1016/j.engstruct.2025.120502
Status : Postprint (Author's version)

investigations have been conducted to derive the S-N curve for a section at mid-span with a support that restrained vertical displacements on the web, for a downward and upward loading. To reach the objective, global and local fatigue tests were performed.

This paper presents experimental investigations conducted on the fatigue resistance of Z-rail members used in multi-deep rack storage structures, loaded by the movements of the shuttle on their lower flanges. The performed experimental campaign includes 34 fatigue tests which were carried out on two specific structural details (mid-span and support details) and subjected to different constant load variations applied to the lower flange of the Z section rail. Through the measured stress ranges, the test results were interpretated to derive an S-N curve to be used for the fatigue design of these details, following the philosophy of prEN1993–1–9. Section 2 summarizes the details of the experimental campaign. Then, the studies conducted for the first and the second structural detail are reported in Section 3 and Section 4, respectively. Finally, the obtained results for both structural details are discussed in Section 5 and compared with those available in the literature. This research is part of a Walloon region project, with the acronym ACTIONS (convention N° 8528), involving the industrial partners STOW and GDTech, the private research company CRM group and the University of Liège.

2. Description of the conducted experimental campaign

2.1. Tested specimens

For all the experimental tests, only one section is considered for the studied Z-shaped members made of cold-formed HX420 LAD steel grade; its geometry is illustrated in Fig. 1(a). The investigated Z-rails are produced through roll forming [26]. This section has been identified as one of the most frequently used by the industrial partners of the aforementioned project, amongst a wide range of available cross-sections on the market with heights included between 160 and 220 mm and thicknesses between 2.5 and 3.5 mm. As thin-walled sections are susceptible to local buckling phenomena, the width to thickness ratio (i.e. c/t) is a key parameter influencing their behaviour. The selected profile presents a ratio c/t = 61.15, which is in the mid-range of the available in the market profiles (varying from 42.4 to 71.8). The ratio between the internal radius of the corner and the thickness is R/t = 1.23.

A total of 34 tests were conducted, 18 of which to characterise the fatigue resistance at mid-span of a Z-rail, and 16 to characterise the fatigue resistance at support. For both test configurations, the tests differ from the intensity of the applied load variation. Furthermore, a static test was performed for each configuration. The specificities of each test are detailed in Sections 3 and 4.

2.2. Characterisation of the material

In order to define the actual material properties, tensile coupon tests have been performed. As stated in ISO377 [27], the mechanical properties differ according to the orientation of the extracted coupon

Published in : Engineering (2025), vol. 337, pp. 1–14
DOI: 10. 1016/j.engstruct.2025.120502
Status : Postprint (Author's version)

specimens due to the roll forming technique involving coiling and uncoiling processes. Therefore, six dog-bone specimens have been extracted, two of each one of the following positions: (i) longitudinally on the web (named *AH*), (ii) perpendicular to the longitudinal direction on the web (named *AV*) and (iii) longitudinally in the larger flange (named *S*); the orientation of the specimens *AH* and *AV* is schematized in Fig. 1(b). Those tensile tests have been performed twice.

Tests results, recorded as engineering stress-strain curves are depicted in Fig. 2, while the main mechanical properties are summarized in Table 1. It can be clearly seen that, as expected, the properties are different in the two perpendicular directions, with the longitudinal properties being lower than the vertical ones.

According to prEN 1993–1–3 [28], the nominal longitudinal yield strength for HX420 LAD steel grade is f_y = 400 MPa while its ultimate one is equal to f_u = 450 MPa. The mean measured longitudinal yield strength, equals $f_{y,longitudinal,mean}$ = 438.82 MPa, is 9.7 % higher than the nominal one, while the actual longitudinal ultimate stress $f_{u,longitudinal,mean}$ = 530.75 MPa is 17.55 % higher.

Concerning the effect of residual stresses arising from the rolling process, it was demonstrated in [25] that these do not affect the fatigue life of the detail. Therefore, it was decided to neglect them in the current study.

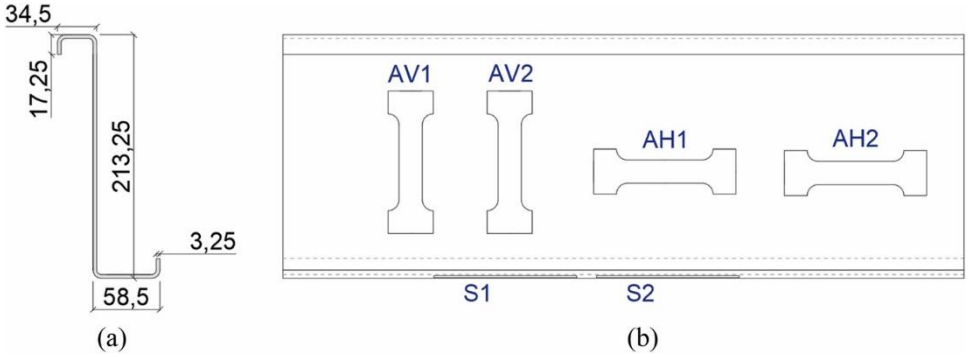

Fig. 1. (a) Z section geometrical properties (in mm) and (b) schematic positions of the specimens for the coupon test

Published in : Engineering (2025), vol. 337, pp. 1–14
DOI: 10. 1016/j.engstruct.2025.120502
Status : Postprint (Author's version)

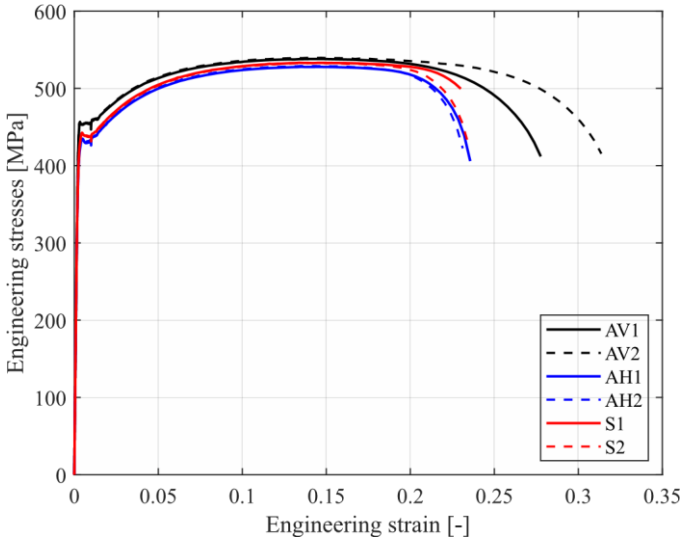

Fig. 2. Stress-strain experimental curves.

Table 1

Actual mechanical properties of HX420 LAD steel grade.

Sample	Elastic strength f_y [MPa]	Ultimate strength f_u [MPa]	Young modulus E [MPa]
AV1	456.7	538.2	204,008
AV2	456.4	539.6	209,514
AH1	434.7	527.9	200,762
AH2	435.5	529.0	202,887
S1	442.6	533.2	203,548
S2	442.5	532.8	194,374
Mean Value	444.7	533.5	202,515

2.3. Setup and instrumentation of "mid-span" tests

The purpose of the first type of experimental tests is to provoke a mid-span fatigue failure in a simply supported Z-rail with a length of 1350 mm, as this section is the most loaded in terms of stresses caused by the bending moment around the strong axis. A schematic 3D drawing view of the test set-up is shown in Fig. 3(a), and a detailed view of one set of two Z-rails is given in Fig. 3(b).

Within a racking structure, the shuttle is running on two rails. In order to reflect this in the laboratory, two Z-rails (green members in Fig. 3(b)) are tested together. To minimize the duration of the experimental campaign, two sub-setups of two Z-rails are tested simultaneously.

The load is applied on the lower flange of the tested rails through an actual wheel coming from a shuttle, located at 9 mm from the web of the profile. This distance is governed by lateral wheels on the side of the shuttle that allows it to circulate perpendicularly to the web of the profile without

Published in : Engineering (2025), vol. 337, pp. 1–14
DOI: 10. 1016/j.engstruct.2025.120502
Status : Postprint (Author's version)

jumping out of the flange. The wheel, made of steel and rubber, has an external diameter of 150 mm and a width of 38 mm. The thickness of the rubber is 10 mm around the circumference.

In order to replicate as closely as possible the loading conditions found in rack structures, the wheels from the shuttle are rigidly connected to a distribution beam, thus simulating the high stiffness of the shuttle (purple in Fig. 3(b)); the jacks are also attached to this beam. Given that, the wheel remains vertical and therefore the torsional deformation is rather limited. In reality, this limitation is ensured by lateral wheels on the shuttle that are in contact with the web of the section, as mentioned above. Additionally, the longitudinal displacement (Y-axis according to Fig. 3(a)) of the wheel is blocked by the restraints applied on the distribution beam.

For each specimen, one support (yellow elements in Fig. 3(b)) is fixed in all displacements (X, Y and Z-axes, according to Fig. 3(a)), while the other one is restrained only about the X and Z-axes. For both supports, the rotation around X-axis is free, while the rotations about Y-axis and Z- axis are restrained due to forks.

In order to reflect the actual support conditions of the Z-rails met in rack structures, as well as to avoid local instabilities due to the reaction forces at the supports during the tests, 30 mm thickness stiffeners (orange pieces in Fig. 3(b)) were placed on each side of the web. The presence of the stiffeners prevents the torsion of the Z-rail at the support, representing thus the actual conditions at the connections of the Z-rails in rack structures.

The load from the jack is applied through load control, with a frequency varying between 1 Hz and 2.5 Hz according to the intensity of the applied load cycles.

Throughout the fatigue test, the applied load was measured using a reaction cell placed at the level of the jack, while the displacement was obtained directly from the jack. In addition, strain gauges measuring the deformations in two perpendicular directions have been installed at the mid-span section for some specimens. The strain gauges were placed at the section of the member where the force is applied. Over the section, the position of the measuring sensors was determined numerically. As a consequence, the two bi-directional strain gauges have been placed on the external face of the Z section just next to the corner, as detailed in Fig. 4(b) by the red square. The specimens *MS1-MS4, MS15-MS18* were instrumented to monitor the crack initiation and the impact on the stress distribution.

Published in : Engineering (2025), vol. 337, pp. 1–14
DOI: 10. 1016/j.engstruct.2025.120502
Status : Postprint (Author's version)

2.4. Set-up of "support" tests

This fatigue tests at the support, schematized in Fig. 5, aims to reproduce the situation when the Z-rail is subjected to the maximum negative bending moment caused by the shuttle wheels, which are on both sides of the support. The 1500 mm length Z-rail is supported by a Σ 200/80/2500 mm length profile, also made of HX420 LAD steel grade (see Fig. 6). Both profiles are connected through a short angle that is bolted on each profile's web; the holes on the Z member are slotted, while, on the Σ member, they are classical rounded ones.

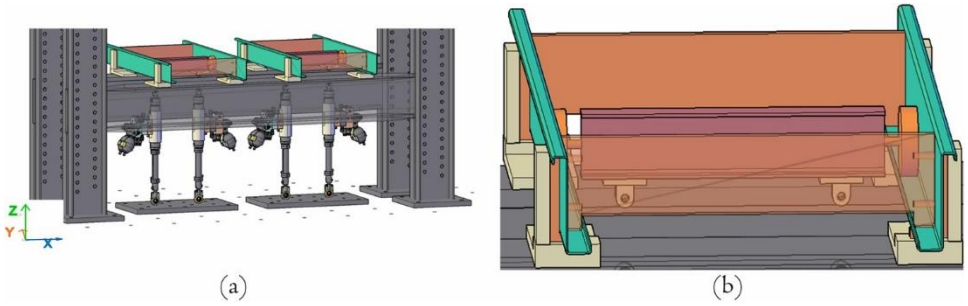

Fig. 3. (a) Mid-span tests 3D global view and (b) set of two Z-rails.

Fig. 4. Position of the gauges (red square) at the loaded section.

Published in : Engineering (2025), vol. 337, pp. 1–14
DOI: 10. 1016/j.engstruct.2025.120502
Status : Postprint (Author's version)

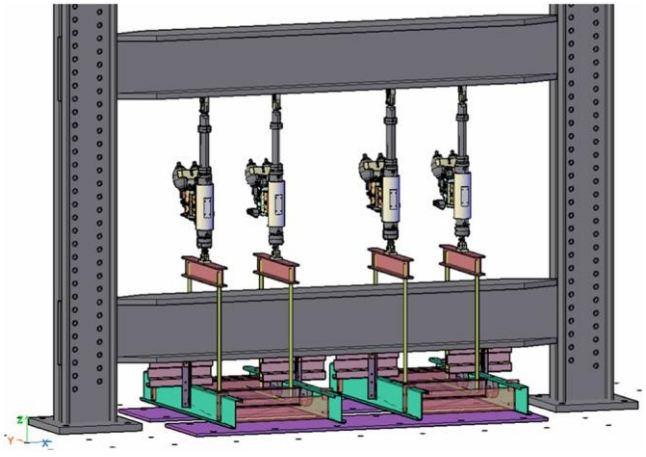

Fig. 5. Tests at support 3D global view.

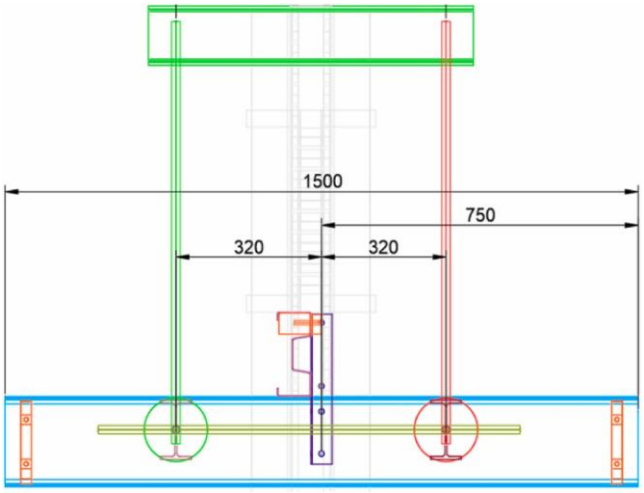

Fig. 6. Transversal view of the test at the support (in mm).

On each side of the Σ-support, a wheel applied a force at 320 mm from the bolts on the Z-rail's web. The same force intensity is applied on each wheel to ensure the equilibrium of the system. At the extremities, the Z-rail section is free to move. The outer face of the bottom flange of the Σ-profile is in contact with the rigid grey beam shown in Fig. 5. Due to the fact that the jack can only pull without the possibility of pushing, the configuration had to be returned as illustrated in Fig. 5. Similarly to the mid-span test, two sub- setups of two Z-rails are tested simultaneously.

As the wheels are located at the same distance from the centre of gravity of the support, the system is theoretically in equilibrium. However, a small perturbation or imperfection in the test set-up would make the system unbalanced. To avoid this, the vertical displacements of the wheels located on the open face side of the Σ beam have been restrained, as shown in Fig. 7 with the distribution beam C1. Thus, the set-up becomes stable without affecting the force distribution. However, to identify any unintentional eccentricity in the system, the support reaction of the fixed wheel is measured by a load cell at the beginning of the tests. A non-zero measured reaction reveals the presence of an

Published in : Engineering (2025), vol. 337, pp. 1–14
DOI: 10. 1016/j.engstruct.2025.120502
Status : Postprint (Author's version)

unintentional eccentricity which requires accordingly the re-adaptation of the test setup. In addition, to reflect the continuity of the Z-member, the displacement along the X-axis and the torsional rotation (around the Y- axis) are blocked at the extremities of the Z-beam by using the same stiffeners as for the mid-span configuration. Finally, the relative displacements in all the directions between the flange of the Σ-support and the rigid grey beam are locked. Similarly to the mid-span tests, the force is applied on the internal lower flange of the rail, by the same type of wheel located at the same distance from the web.

In order to simulate the rigidity of the shuttle and to avoid any relative movement between the wheels, threaded rods (in yellow in Fig. 7) were linked together the two lower distribution beams. To minimise the rotation of the cantilever part of the beam, the tests were carried out by applying the force from $-\Delta P/2$ to $\Delta P/2$ with the reference state which corresponds to $P_{min} + \Delta P/2$.

To avoid local instabilities on the web of the Σ beam, a stiffener is placed between the web and the flange in contact with the supporting beam. Finally, the jacks are controlled by force and the frequency is varying between 1 Hz and 3 Hz.

3. Fatigue at mid-span: experimental results

3.1. Static test

Prior to the fatigue tests, a three-point bending test was carried out so as to investigate the behaviour of these members in this specific configuration, as shown in Fig. 8. The objective of this test was to evaluate the load range intensity to be applied during the high cycle elastic tests. The force was applied in a quasi-static manner until one of the specimens failed. The test was finally stopped due to a slip of the wheel associated to a significant torsional deformation accompanied by a distortional deformation of the section at the position of the applied load, as shown in Fig. 9.

Fig. 10 shows the measured force versus the vertical displacement for this static test. It can be seen that the maximum applied force was

Published in : Engineering (2025), vol. 337, pp. 1–14
DOI: 10. 1016/j.engstruct.2025.120502
Status : Postprint (Author's version)

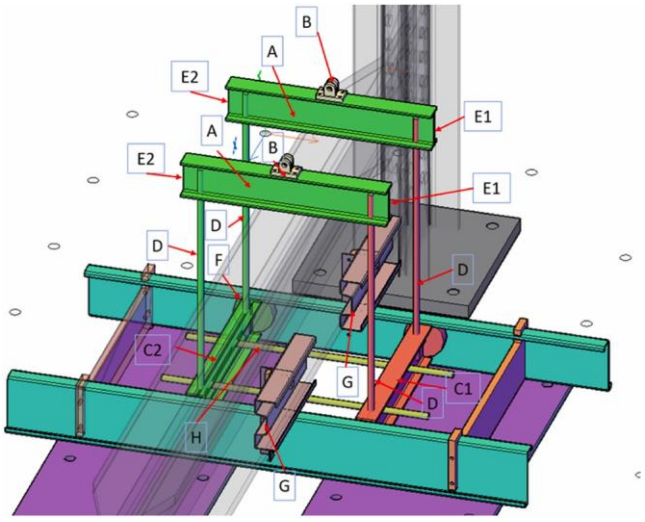

Fig. 7. Transferring of the force from the jack to the Z-rail.

Fig. 8. Photo of the setup of the mid-span test.

Published in : Engineering (2025), vol. 337, pp. 1–14
DOI: 10. 1016/j.engstruct.2025.120502
Status : Postprint (Author's version)

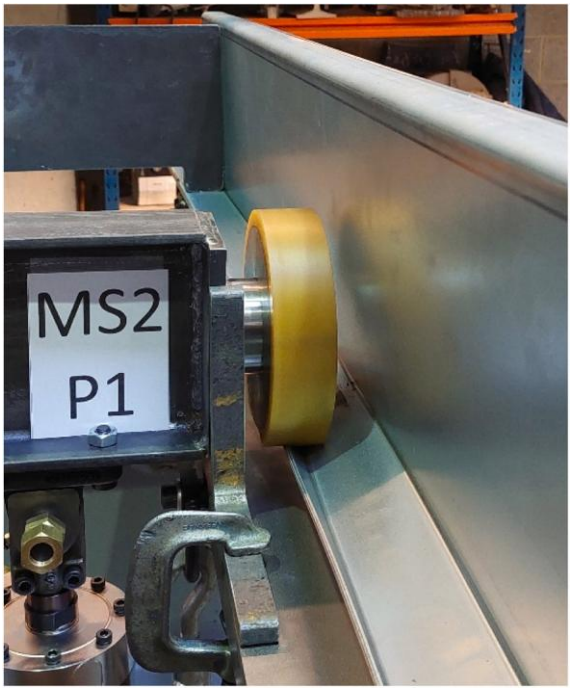

Fig. 9. Failure of the member due to excessive torsional deformation.

22.24 kN for *MS1* and 21.82 kN for *MS2*. The black dashed line in Fig. 10 reflects the initial elastic stiffness of the *MS1* F-u curve. Based on these results, it can be safely assumed that the Z-rail will remain in the elastic range as far as the applied force is not exceeding 11 kN.

3.2. High cycle elastic fatigue tests

In total, 18 specimens (*MS1* to *MS18* – see Table 2) were tested. Amongst them, 16 were subjected to a constant load range varying from ΔP = 3.3 kN to ΔP = 10.1 kN so that no global yielding was reached. The two remaining specimens (*MS5*-*MS6*) were submitted to constant load range higher than 11 kN in order to investigate the fatigue behaviour of the beam against a high load range involving local yielding. From a practical point of view, it can be deduced that the shuttle transfers the pallet load using four wheels. Considering a total weight of 2000 kg [29], each wheel transfers 4.9 kN. It should be noted that high loads do not reflect actual loading conditions; such load levels allow to obtain points to be reported in the S-N curve for a high stress range. In agreement with Masendorf et al. [30], who refer to DIN50100, the entire experimental campaign was performed by considering a constant load ratio of $\frac{P_{max}}{P_{min}}$ = 10. Table 2 summarizes for each specimen the applied load range, the associated maximum and minimum loads, as well as the number of cycles when the tests were stopped and the number of cycles corresponding to an increase of 10 % of the specimen displacement (see explanations here after). The vertical displacement of the jack, the number of cycles and the load range were recorded throughout all the tests.

Published in : Engineering (2025), vol. 337, pp. 1–14
DOI: 10. 1016/j.engstruct.2025.120502
Status : Postprint (Author's version)

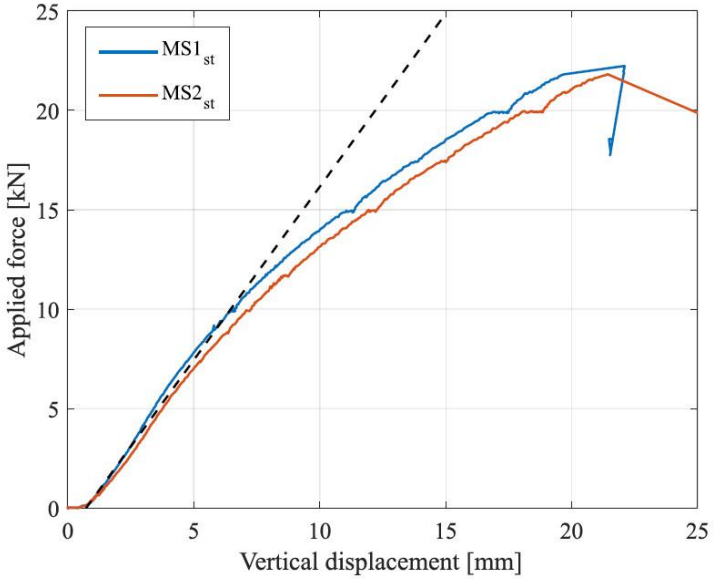

Fig. 10. Mid-span quasi-static test results.

Among the 18 fatigue tests, 8 leads to run out, meaning that no fatigue failure appeared even after a large number of cycles. Furthermore, it was observed that, in specimens *MS13* to *MS16* subjected to the same load range, fatigue cracks developed in two Z-rails (*MS13-MS14*), while, such cracks were not observed in specimens *MS15-MS16*, even after a consequent number of cycles. This can be explained by the material structure of the steel, as this parameter is a leading one in the fatigue behaviour [31]. Similar observations can be found in the literature [32], [33] and [34]. As the tests were running continuously, it was almost impossible to determine the number of cycles for which the crack developed. Moreover, for safety reasons, as the tests were force controlled, a displacement limit was imposed to avoid the failure of the entire system. Therefore, as no specific criterion to identify the number of cycles associated to the fatigue failure is proposed in the literature, the following one was established: the number of cycles reported in the S-N curve diagram, as a result from the fatigue test, was derived to correspond to a 10 % increase of the specimen displacement. The application of this criterion is illustrated hereafter for the *MS9* specimen. Fig. 11 presents the number of cycles versus the maximum and minimum displacement for the *MS9* specimen; the difference between the minimum and maximum displacements is also reported. It can be seen that from 0 to 130,000 cycles, the displacement range remains almost constant at 3.31 mm; an increase of 10 % of this displacement would be equal to 3.64 mm. Plotting this value on the graph (dashed red line), the intersection with the displacement range curve gives a number of cycles equal to 201,380 cycles. The same procedure is applied for all specimens when a fatigue crack is developed and the number of cycles to consider is reported in Table 2.

Concerning the pattern of the fatigue crack, for all specimens for which a fatigue failure occurred, the crack initiates along the inner corner between the flange on which the force is applied and the web of the section. The crack then progresses towards the outer corner and once fully developed through the

Published in : Engineering (2025), vol. 337, pp. 1–14
DOI: 10. 1016/j.engstruct.2025.120502
Status : Postprint (Author's version)

thickness, propagates towards the extremities of the specimens. This evolution is shown in Fig. 12(a) and (b), for the *MS9* sample and *MS15* respectively, for which it was possible to monitor the development of the crack. This highlights that local stresses responsible for the crack development and propagation are not the ones associated to the bending moment, but the transversal stresses resulting from the relative opening of the flange compared to the web of the profile.

Table 2

Results of the mid-span test campaign.

Specimen	ΔP [N]	*P*min [N]	*P*max [N]	Δσ [MPa]	Number of cycles – Tests sopped	Number of cycles – 10 % difference
MS1	3328.43	373.44	3701.87	171.17	Run out	
MS2	3337.34	357.70	3695.04	171.63	(2,800,000)	
MS3	3333.69	376.87	3710.55	171.44		
MS4	3331.43	366.78	3698.22	171.33		
MS11	3872.22	409.67	4281.89	199.14	Run out	
MS12	3897.08	403.18	4300.26	200.42	(6,500,000)	
MS13	4554.94	527.35	5082.29	234.25	1,274,345	1,055,150
MS14	4579.58	501.17	5080.75	235.52		1,212,622
MS15	4595.58	498.17	5094.09	236.36	Run out	
MS16	4598.27	494.42	5092.69	236.48	(3,500,000)	
MS9	5981.45	669.96	6651.41	307.61	290,536	201,380
MS10	5955.28	689.69	6641.97	306.26		226,575
MS7	9868.96	1129.43	10,998.39	507.54	36,613	27,563
MS8	9901.78	1159.94	11,061.71	509.22		27,563
MS17	10,070.84	1057.56	11,128.4	517.92	30,079	24,622
MS18	9964.85	1126.3	11,090.88	512.47		27,245
MS5	14,775.72	1784.11	16,559.83	759.88	7,792	5,866
MS6	14,815.11	1784.06	16,559.17	761.91		5,416

Published in : Engineering (2025), vol. 337, pp. 1–14
DOI: 10. 1016/j.engstruct.2025.120502
Status : Postprint (Author's version)

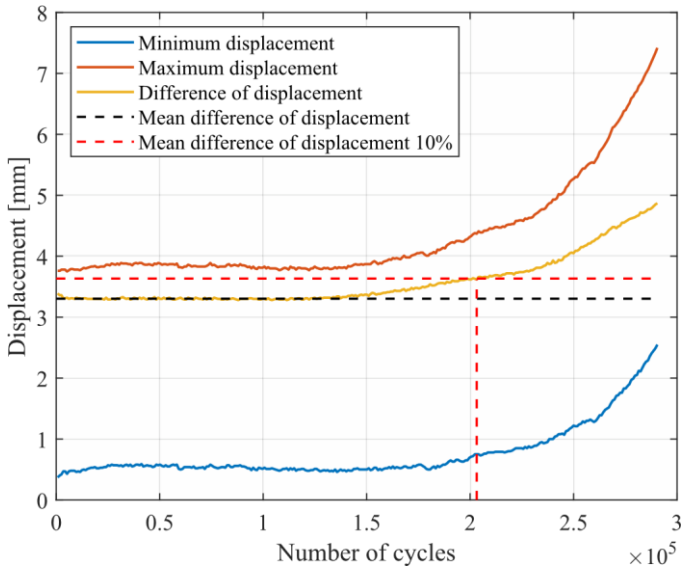

Fig. 11. Number of cycles derivation criterion for the *MS9* specimen.

As it was not possible to record the strain all along the test, the strains were measured after some specific number of cycles by stopping the test, loading the rails in a quasi-static manner and then re-launching the fatigue test. Fig. 13 shows the curves that link the vertical displacement with the measured micro strains for the *MS18* specimen. It should be noticed that a small perturbation is caught through the measurement of the horizontal strain on the web at 20,205 cycles (yellow curve in Fig. 13 (b)), which seems to indicate that a crack was initiated, even if not yet visible to the eye; indeed, the crack was only visible around 21,750 cycles. Similar curves were obtained for specimen *MS17* but are not reported here, while for the other specimens for which no fatigue crack developed, the curves were exactly the same as the blue one (0 cycles) in Fig. 13.

It can be observed that as the number of cycles increases above 15,000 cycles, the strain in the vertical direction on the web is decreasing, leading thus to a reduction of the stresses, and highlighting a loss of rigidity of the rail. On the contrary, the strain in the flange along the longitudinal direction and the associated stress are increasing.

Published in : Engineering (2025), vol. 337, pp. 1–14
DOI: 10. 1016/j.engstruct.2025.120502
Status : Postprint (Author's version)

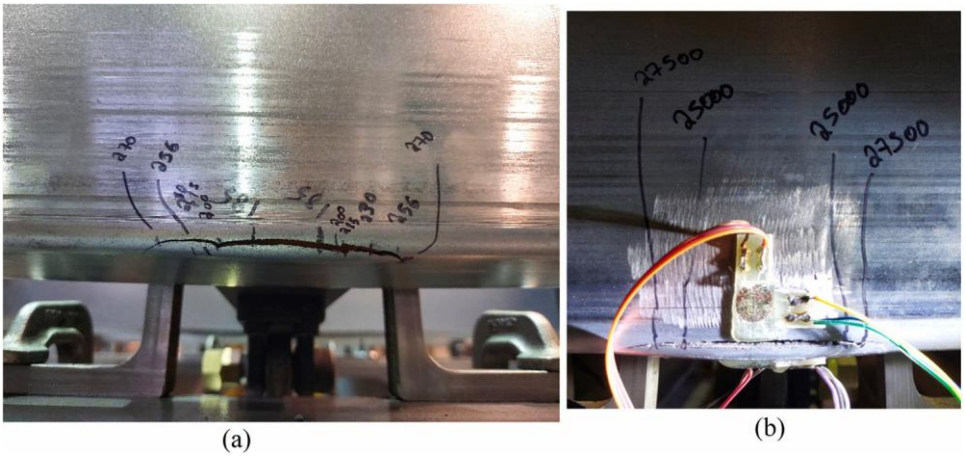

Fig. 12. Fatigue crack pattern for (a) *MS9* specimens, number of cycles to be multiplied by 10^3 and (b) *MS15* specimens.

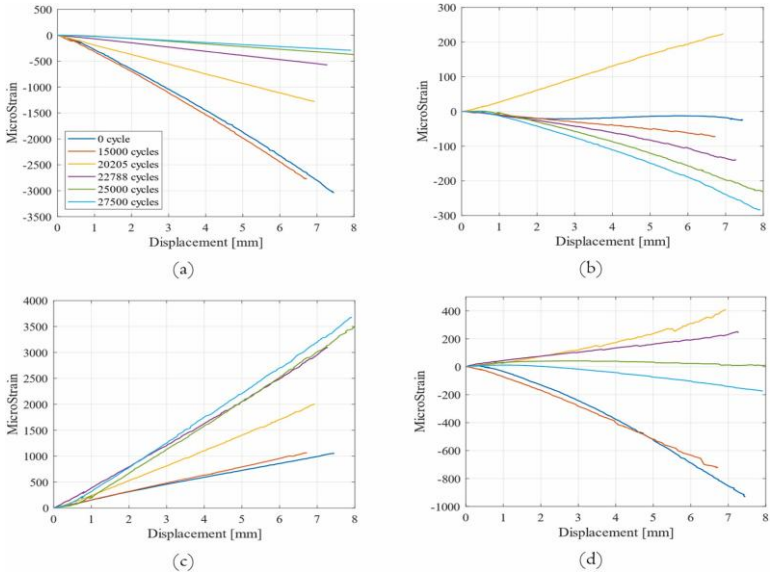

Fig. 13. Strain curves for specimen MS18 versus displacement (a) vertically on the web, (b) horizontally on the web, (c) longitudinally on the flange and (d) transverse direction on the flange.

Published in : Engineering (2025), vol. 337, pp. 1–14
DOI: 10. 1016/j.engstruct.2025.120502
Status : Postprint (Author's version)

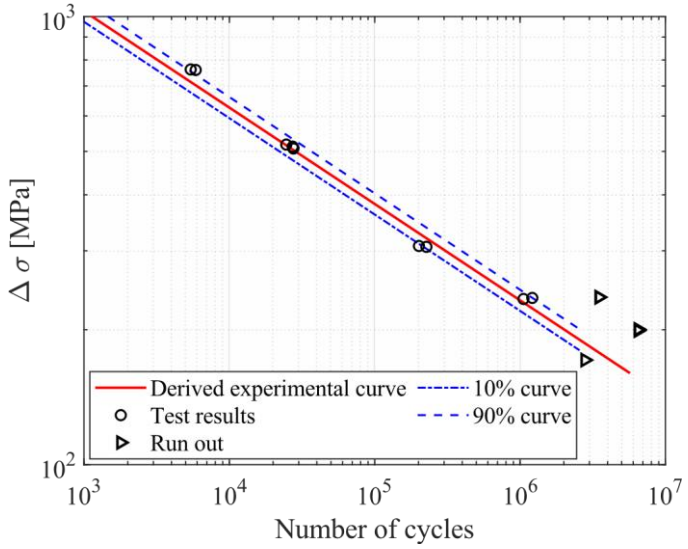

Fig. 14. Derived S-N curve for the mid-span detail.

The experimental results reported in Fig. 14 were derived by computing the stress variation from the strains measured in the non- damaged initial state (number of cycle = 0) of the specimen through the vertical gauge placed on the web. This gauge was selected as a reference, as it was the closest one to the crack initiation; the strain was converted into stress by using the Hook Law (E = 206,761 MPa, mean value between *AV1* and *AV2* results tensile tests), as reported in Table 3. The force intensities ($P_{i,st}$) given in this table are the applied ones recorded during the registration of the strain. These forces are differing from the values reported in Table 2 as the latter correspond to the mean extreme forces measured during the entire fatigue test.

Subsequently, to extrapolate the results for the other specimens that were not instrumented with strain gauges, the absolute mean value of the ratio between the applied force and the induced stress ($\Delta P/\Delta\sigma$ = 19.44) is computed. As the strain gauge was placed on the outer part of the corner and measuring then compressive stresses, the absolute value has been used. In addition, it should be noted that the value of these stress ranges are not the ones responsible for fatigue as the measures have been taken on the opposite face of the crack initiation. However, the latter stress ranges are good indicators of the stress variations on the opposite face, considering that the specimen remain in the elastic range prior to the development of the fatigue crack. Finally, by applying Eq. 1, the stress ranges for the other specimens can be extrapolated; the latter are reported in Table 2.

$$\Delta\sigma = \frac{\Delta P}{19.44} \tag{1}$$

In order to define, from the experimental results, the slope of the S-N curve, the pearl string method provided in DIN50100 [35] has been applied, considering all the tests except the run-out ones (i.e.

Published in : Engineering (2025), vol. 337, pp. 1–14
DOI: 10. 1016/j.engstruct.2025.120502
Status : Postprint (Author's version)

MS1-MS4, MS11-MS12, MS15-MS16) and the yielded ones (*MS5-MS6*). The S-N curve is obtained by applying Eq. 2:

$$N = C \cdot \Delta\sigma^{-m} \quad (2)$$

where *m* (the slope) and *C* are constants and can be obtained by:

$$m = \frac{n \cdot \sum(log\Delta\sigma_i \cdot logN_i) - \sum(log\Delta\sigma_i) \cdot \sum(logN_i)}{n \cdot \sum((log\Delta\sigma_i)^2) - (\sum(log\Delta\sigma_i))^2} = 4.6508 \quad (3)$$

$$C = 10^{\frac{1}{n} \cdot (\sum(logN_i) + m \cdot \sum(log\Delta\sigma_i))} = 1.0167 \cdot 10^{17} \quad (4)$$

with *n* (= 8) the total number of considered results.

Table 3 Computed induced stress.

Specimen	$P_{Min,st}$ [N]	$P_{Max,st}$ [N]	ΔP_{st}[N]	σ_{Min} [MPa]	σ_{Max} [MPa]	Δσ [MPa]	$\left\|\frac{\Delta P}{\Delta\sigma}\right\|$
MS1	4.55	3707.75	3703.2	0	− 179.42	− 179.42	20.64
MS2	0.65	3688.25	3687.6	0	− 187.27	− 187.27	19.70
MS3	3.18	3719.51	3716.33	0	− 196.28	− 196.28	18.93
MS4	4.05	3734.23	3730.19	0	− 170.54	− 170.54	21.87
MS13	0.67	5003.64	5002.97	0	− 273.38	− 273.38	18.3
MS14	5.34	5121.49	5116.15	0	− 252.36	− 252.36	20.27
MS17	0.01	11,158.9	11,158.9	0	− 601.64	− 601.64	18.54
MS18	0.52	11,087.7	11,087.2	0	− 640.87	− 640.87	17.3

As a comparison, the 10 % criterion that allows to determine the number of cycles to be reported on the S-N curve, has been chosen after a comparison of different values, respectively 5 %, 10 % and 15 %. Exceeding this level of deformation would result in significant displacement, making the movement of the shuttle on the rail impossible. Slope *m* for a criterion of 5% is equal to $m_{5\%}$ = 4.68 while for 15 %, is $m_{15\%}$ = 4.44. The results obtained for 5 % are closed to the ones computed for 10 %, while the slope obtaining with 15 % criterion is too far from the two other values.

Published in : Engineering (2025), vol. 337, pp. 1–14
DOI: 10. 1016/j.engstruct.2025.120502
Status : Postprint (Author's version)

To assess the accuracy of the test results, the standard deviation $\tilde{S}_{logN}$ is computed by applying the DIN50100 which assumes that it does not vary between the different stress ranges. Therefore, to calculate the standard deviation, a fictitiously stress range is considered and the test results are shifted parallel to the derived curve, to obtain the associated fictitious number of cycles $N_{i,fict}$ evaluated by Eq. 5:

$$N_{i,fict} = N_i \cdot \left(\frac{\Delta\sigma_{fict}}{\Delta\sigma_i}\right)^{-m} \quad (5)$$

Then, the mean value of the number of cycles, $N_{50\%,fict}$ is given by Eq. 6:

$$N_{50\%,fict} = 10^{\frac{1}{n}\sum logN_{i,fict}} \quad (6)$$

and the standard deviation by Eq. 7:

$$\tilde{S}_{logN} = \sqrt{\left(\frac{1}{n-2}\right) \cdot \sum_{i=1}^{n} (logN_{i,fict} - logN_{50\%,fict})^2} \quad (7)$$

Given that the sample size is rather small, the standard deviation has been corrected by applying Eq. 8:

$$\tilde{S}_{logN_{corr}} = \tilde{S}_{logN} \cdot \frac{n-1.74}{n-2} \quad (8)$$

Table 4

Statistical evaluation of the results for the mid-span test.

Specimen	$\Delta\sigma$ [MPa]	$N_{i,fict}$	$\log N_{i,fict}$	$(\log N_{i,fict} - \log N_{50\%,fict})^2$
MS13	234.25	87,610.448	4.943	0.001
MS14	235.52	103,249.546	5.014	0.01
MS9	307.61	59,367.186	4.774	0.02
MS10	306.26	65,442.256	4.816	0.01
MS7	507.54	83,419.700	4.921	0
MS8	509.22	84,711.695	4.928	0
MS17	517.92	81,876.134	4.913	0
MS18	512.47	86,248.961	4.936	0
MS5	759.88	115,999.109	5.064	0.02
MS6	761.91	108,437.616	5.035	0.02

The standard deviation was computed considering a fictitious stress range of $\Delta\sigma$ = 400 MPa; the details are given in Table 4 and $\tilde{S}_{logN_{corr}}$ is equal to 0.085.

Published in : Engineering (2025), vol. 337, pp. 1–14
DOI: 10. 1016/j.engstruct.2025.120502
Status : Postprint (Author's version)

In addition, the scatter bands are calculated for a failure probability of 10% and of 90%, using the same slope *m* and for a number of cycles obtained by:

$$N_{10\%,fict} = 10^{logN_{50\%,fict} - 1.282 \cdot \tilde{s}_{logN,corr}} \quad (9)$$

$$N_{90\%,fict} = 10^{logN_{50\%,fict} - 1.282 \cdot \tilde{s}_{logN,corr}} \quad (10)$$

Those curves are plotted in Fig. 14 and it can be easily seen that the interval between them is very limited.

The slope that equals m = 4.65, is close to the one proposed by prEN1993–1–9 (m = 5).

4. Fatigue at the support: experimental results

4.1. Static test

As for the mid-span tests, a static test was performed on the Z-rail in the specific configuration shown in Fig. 16(a) and Fig. 16(b), subjected to point loads. The jack applied in a quasi-static manner a force varying from 0 to 25 kN, by making an unloading to 1 kN for each 5 kN step. In addition to the vertical displacement recorded at the level of the jack, the reaction force was also measured by the load cell shown in Fig. 16(c), to verify the equilibrium of the system. The graph in Fig. 15(a) presents the force - vertical displacement curve, while Fig. 15(b) provides the graph relating the reaction force versus the applied force.

It can be observed that the Z-rail remains in the elastic zone for load intensity up to 25 kN, as no real inflexion point appears in the curve. Furthermore, due to the maximum limitation of the jack, the failure was not reached. During the loading of the beam, the reaction force remains quite small, i.e. less than 0.25 kN for the maximum applied load. It can be therefore concluded that the system is equilibrated. Finally, it has to be mentioned that no cracks and local yielding were visually observed during the test.

4.2. High cycle elastic fatigue tests

The fatigue resistance of the second detail, at the support, was studied by performing 16 fatigue tests with constant load ranges varying from ΔP = 7.52 kN to ΔP = 18.05 kN, for which the members remained globally in the elastic zone. The load range, the associated minimum and maximum load and the number of cycles after which the jacks stopped are detailed for each specimen in Table 5. As for the previous detail, the vertical displacement and the applied force are recorded all along the cyclic test and the reaction force is measured through a quasi-static test before starting the fatigue loading.

Published in : Engineering (2025), vol. 337, pp. 1–14
DOI: 10. 1016/j.engstruct.2025.120502
Status : Postprint (Author's version)

Within the 16 tested members, one set of two Z-rails never cracked, even after a high number of cycles. The results for specimens *S9* to *S14* are quite scattered, as for tests *MS13* to *MS16* performed on the previous detail, this could be explained by the microstructure of the steel that was different for the *S11-S12* specimen compared to the other rails. Similarly to the tests at mid-span, the number of cycles reported in the S-N curve represents the number of cycles for which the 10 % difference in displacement is reached.

For this test series, a fatigue crack was expected at the section of the Z-rail over the Σ-element. However, the crack finally appears first at the section where the fixed wheel applies the force, in the corner between the flange and the web of the section (see Fig. 17); the crack pattern being the same as for the mid-span tests. For specimen *S9*, the crack appeared at two positions: first at the section where the wheel is fixed in displacement and then at the position where the vertical displacement of the wheel is allowed.

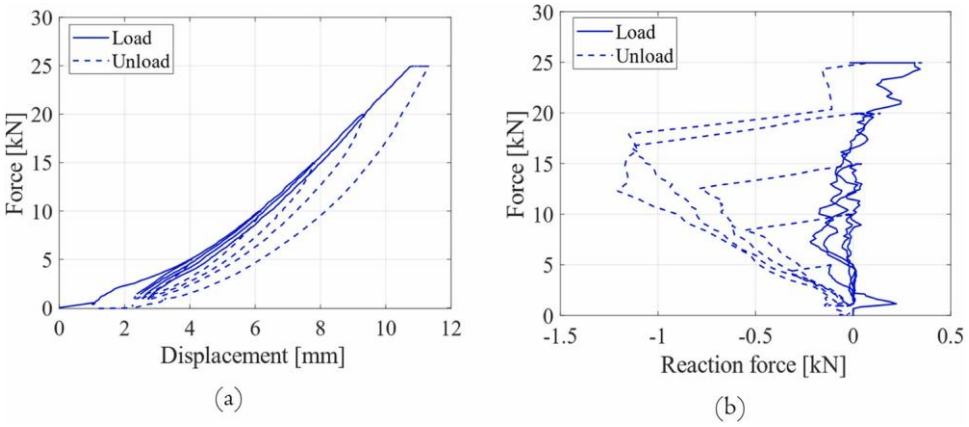

Fig. 15. Measured data from the support static test (a) force - vertical displacement curve and (b) force - reaction force curve.

Published in : Engineering (2025), vol. 337, pp. 1–14
DOI: 10. 1016/j.engstruct.2025.120502
Status : Postprint (Author's version)

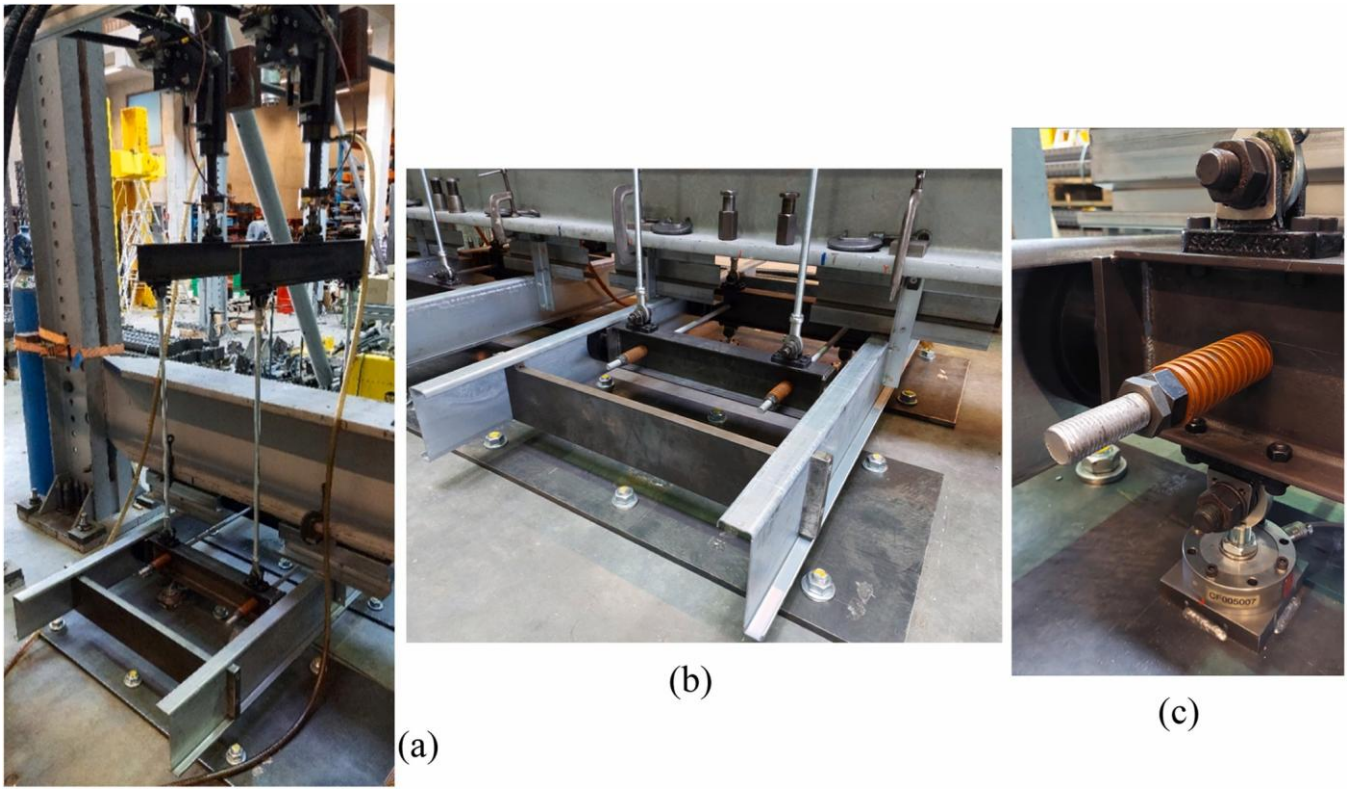

Fig. 16. Detailed view of (a) the test set-up for the support detail (b) the tested specimens and (c) the load reaction cell.

For the monitoring of the crack evolution, two strain gauges were placed in the two main perpendicular directions on Z-rails *S15* and *S16*

(ΔP = 18 kN), at the level of the load application sections, as represented in Fig. 4. The gauges were installed at the same position as for the mid-span tests. The measurements were recorded for some specific number of cycles, by stopping the fatigue test to apply the force in a quasi-static manner for a few cycles, before launching again the cyclic test.

Fig. 18 highlights the apparition of the crack firstly at the level of the fixed wheel section, as the stress range starts to change after 30,000 cycles whereas at the free displacement section the stresses do not differ until 40,000 cycles. The same redistribution of stresses across the section appears also here; the stress range increases in the longitudinal direction on the flange as the number of cycles raises, while it decreases on the web. It can be seen from the curves that, during the same loading/ unloading period, the sign of the recorded stress is changing; this is due to the fact that the load varies between $\pm \Delta P/2$ so as to avoid the effect of a too high rotation of the Z-rail on the support, caused by the bending of the cantilever part of the beam due to the fixed vertical displacement at one extremity. The initial state corresponds to a load of $P_{min} + \Delta P/2$, already applied on the rail; in Fig. 18, this applied load is equal to ~10.9 kN with P_{min} equal to ~1.9 kN and ΔP equal to ~18 kN.

Published in : Engineering (2025), vol. 337, pp. 1–14
DOI: 10. 1016/j.engstruct.2025.120502
Status : Postprint (Author's version)

The determination of the stress range applied on the Z-rail to report in the S-N curve is based on the strain measured by the vertically placed gauge on the web, converted using the Law of Hook (E = 206,761 MPa). The resulting values extracted from the four vertical devices are provided in Table 6, while the ratio between the load range and the stress ranges for which the computed absolute mean value is $\Delta P/\Delta\sigma = 47.52$ are reported too.

Table 5
Results of the test support campaign.

Specimen	ΔP [N] (Jack)	*P*min [N] (Jack)	*P*max [N] (Jack)	Δσ [MPa] (Wheel)	Number of cycles – Tests sopped	Number of cycles – 10 % difference
S7	7518.11	874.87	8392.98	158.20		2,802,275
S8	7567.19	758.98	8326.12	159.23		(Run out)
S11	9675.81	1135.48	10,811.30	203.60	643,399	545,184
S12	9575.32	1193.39	10,768.39	201.48		589,977
S9	9689.45	1190.8	10,880.26	203.88	1,039,599	916,020
S10	9695.25	1163.28	10,858.53	204.01		962,212
S13	9740.25	1138.42	10,878.67	204.95	1,330,907	1,246,447
S14	9798.94	1171.23	10,970.17	206.19		1,154,462
S3	12,545.83	1427.22	13,973.05	263.99	177,968	138,737
S4	12,511.26	1494.92	14,006.18	263.26		128,989
S5	12,729.11	1420.13	14,149.24	267.84	313,364	195,784
S6	12,698.29	1413.02	14,111.31	267.20		179,887
S1	17,887.40	2075.09	19,969.49	376.38	51,490	50,922
S2	17,887.40	2075.09	19,699.49	376.38		48,522
S15	18,055.12	1984.02	20,039.14	379.91	58,126	43,565
S16	18,001.91	2023.44	20,025.35	378.79		37,026

Published in : Engineering (2025), vol. 337, pp. 1–14
DOI: 10. 1016/j.engstruct.2025.120502
Status : Postprint (Author's version)

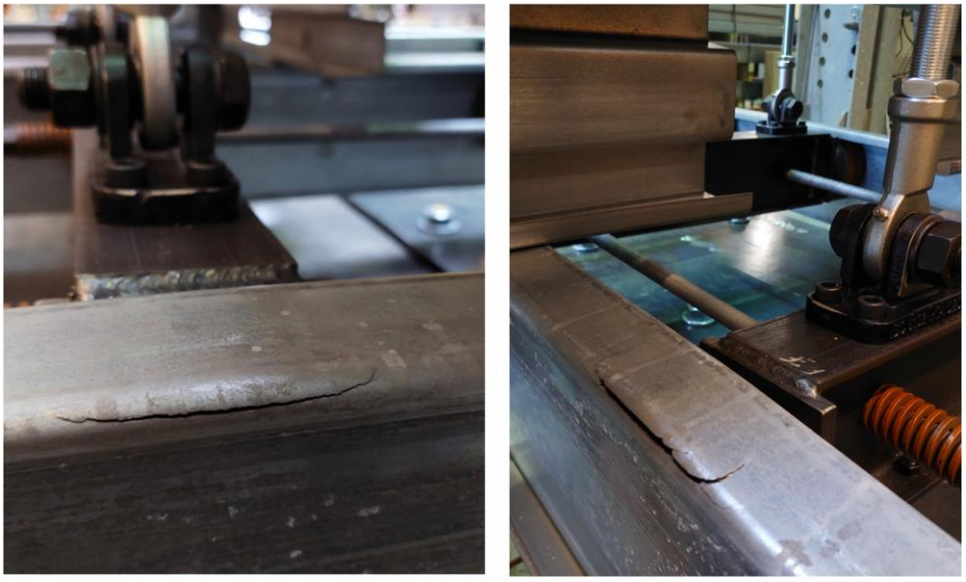

Fig. 17. Fatigue crack for (a) specimen *S2* and (b) specimen *S4*.

Then, based on Eq.11, the stress range is extrapolated for the 14 other specimens, and the computed results are given in Table 5.

$$\Delta\sigma = \frac{\Delta P}{47.52} \tag{11}$$

The constant *m* and *C* are again computed using Eq.2 and applying the pearl string method; the parameters *m* = 4.8 and *C* = $9.4341 \cdot 10^{16}$ are obtained through Eq.3 and Eq.4, respectively. The associated S-N curve is plotted in Fig. 19.

The accuracy of the test results has been evaluated by computing the standard deviation $\tilde{S}_{logN}$, using Eq. 5 to Eq. 8, considering a fictitiously stress range of $\Delta\sigma$ = 400 MPa. The standard deviation is therefore equal to $\tilde{S}_{logN,corr}$ = 0.1574 and details are provided in Table 7.

Moreover, the scatter bands for a failure probability of 10 % and of 90 % are plotted in Fig. 19 using the determined slope *m* and for the number of cycles at 50 % probability, applying Eq.9 and Eq. 10.

5. Comparisons and discussions

5.1. Comparison of the test results for both studied details

By analysing the results of both details, which consist of a section of the Z-rail subjected to punctual load applied by a wheel, it can be concluded that the fatigue weakness of the Z-rail is the same, i.e.

Published in : Engineering (2025), vol. 337, pp. 1–14
DOI: 10. 1016/j.engstruct.2025.120502
Status : Postprint (Author's version)

the rounded corner between the flange and the web, in which a longitudinal crack developed caused by the relative opening of the flange. More precisely, a crack appears just at the rounded corner between the flange and the web, and propagates longitudinally towards the extremities of the member. As the crack pattern and the fatigue weak position are the same, all the results are plotted in a single graph presented in Fig. 20(a).

Fig. 20(a) shows that the computed slope of the support detail ($m_{support}$ = 4.8) is closer to the one proposed by prEN1993–1–9 ($m_{prEN1993\text{-}1\text{-}9}$ = 5), compared to the slope resulting from the mid-span detail ($m_{midspan}$ = 4.65). On the contrary, the scatter bands for the mid- span detail are closer than for the support one. By computing the slope of the curve considering all the data at the same time, the results (m_{all} = 4.04) are lower than by considering both types individually.

This could be explained by the fact that for the same stress range according to the S-N curve, the support detail has a lower resistance than the mid-span one, so the disparity is higher. However, for the same applied load, the resulting stress in the support detail is lower than the one for mid-span detail. This can be related to the continuity of the rail for the mid-span case from both sides of the wheel but not for the support detail where the extremity of the rail is free to move. This leads for the same applied load range to lower displacement and so to higher stresses in the first case, and by consequence to a lower fatigue resistance. As a conclusion, for the same load range, the fatigue life is quite similar, as it is justified by the graph in Fig. 20(b) that links the applied load ranges with the number of cycles. As in the rack storage structure, the static scheme of the Z-rails is typically characterised by its continuity over the support, the mid-span test results curve should be used, given that it has been shown that the support tests results do not reflect accurately the reality. Such members should be then designed against fatigue using the mid-span curve (Fig. 14) and by computing the stress range according to Eq. 1 (structural hot spot method).

Published in : Engineering (2025), vol. 337, pp. 1–14
DOI: 10. 1016/j.engstruct.2025.120502
Status : Postprint (Author's version)

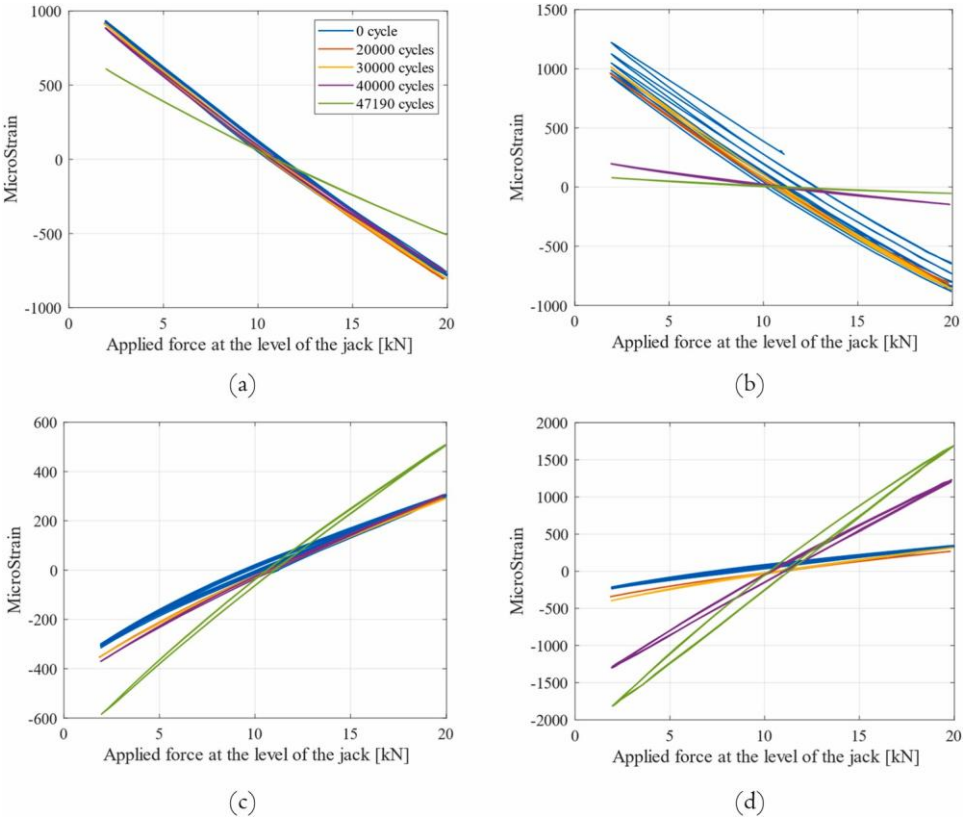

Fig. 18. Strain measured from *S15* specimens (a) vertical direction on the web at the free wheel section, (b) vertical direction on the web at the restrained wheel section, (c) longitudinal direction on the flange at the free wheel section and (d) longitudinal direction on the flange at the fixed wheel section.

Table 6

Applied force and derived stress range measurement for support detail.

Specimen	*PMin,st*[*N*]	*PMax,st*[*N*]	ΔP_{st} [N]	*σMin* [MPa]	*σMax* [MPa]	Δσ [MPa]	$\left\lvert\frac{\Delta P}{\Delta \sigma}\right\rvert$
S15 (fixed side)	1931.01	19,950.54	18,019.53	− 134.09	252.43	386.51	46.62
S16 (fixed side)	1908.2	19,973.58	18,065.38	− 183.62	204.64	388.26	46.52
S15 (free side)	1931.01	19,950.54	18,019.53	− 161.99	189.92	351.90	51.21
S16 (free side)	1908.2	19,973.58	18,065.38	− 198.9	198.90	394.94	45.74

Published in : Engineering (2025), vol. 337, pp. 1–14
DOI: 10. 1016/j.engstruct.2025.120502
Status : Postprint (Author's version)

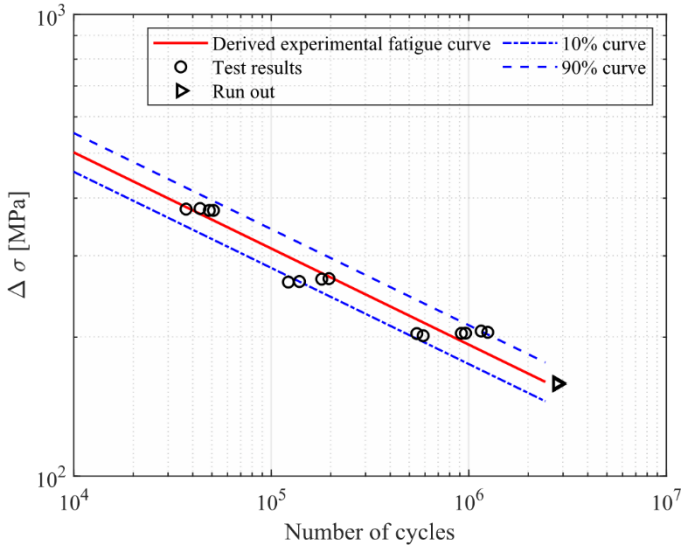

Fig. 19. Derived S-N curve for the support detail.

Table 7

Statistical evaluation for the support test.

Specimen	Δσ [Mpa]	$N_{i,fict}$	log$N_{i,fict}$	(log$N_{i,fict}$ – log$N_{50\%,fict}$)^2
S11	203.60	21,270.90	4.33	0.01
S12	201.48	21,781.35	4.34	0.01
S9	203.88	35,982.05	4.56	0.02
S10	204.01	37,905.24	4.58	0.03
S13	204.95	50,206.94	4.70	0.09
S14	206.19	47,863.07	4.68	0.08
S3	263.99	18,849.79	4.27	0.01
S4	263.26	17,294.60	4.24	0.03
S5	267.84	28,519.77	4.45	0.01
S6	267.20	25,900.71	4.41	0
S1	376.38	38,015.49	4.58	0.03
S2	376.38	36,223.78	4.56	0.03
S15	379.91	34,014.30	4.53	0.02
S16	378.79	28,501.90	4.45	0.01

Published in : Engineering (2025), vol. 337, pp. 1–14
DOI: 10. 1016/j.engstruct.2025.120502
Status : Postprint (Author's version)

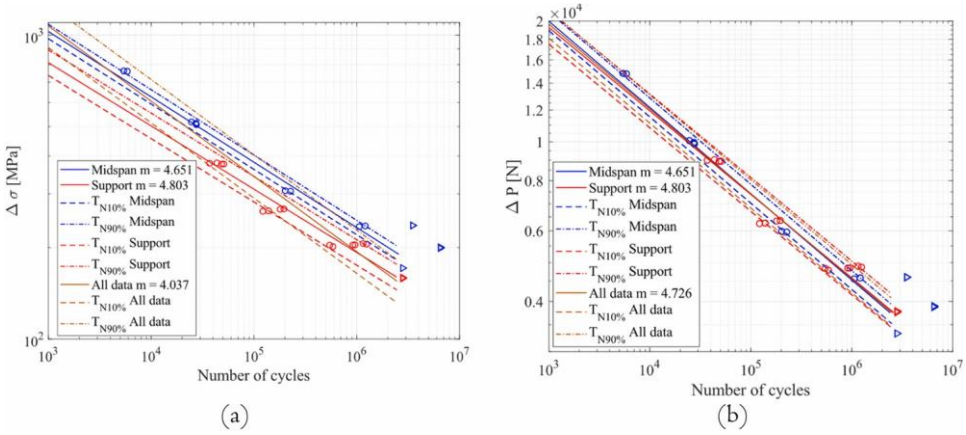

Fig. 20. Comparison of the results for the two details in terms of (a) stress range (b) load range.

5.2. Comparison of the test results with the outcomes of the fastcold project

The experimental results obtained in the current research project have been compared to the ones of the FASTCOLD project [25]. Fig. 21 presents the S-N curve resulting from the stress ranges derived for the 18 fatigue tests performed for the downward loading situation compared to the two ones obtained in the current study. The stress ranges reported in the FASTCOLD project are computed based on a numerical model reflecting the experimental conditions using Abaqus software, considering the maximum principal stress at the crack location. Moreover, in the FASTCOLD project it is considered that the number of cycles to be reported in the S-N curve corresponds to a decreasing of 10 % in the stress range measured by strain gauges at the level of the inner corner between the flange and the web.

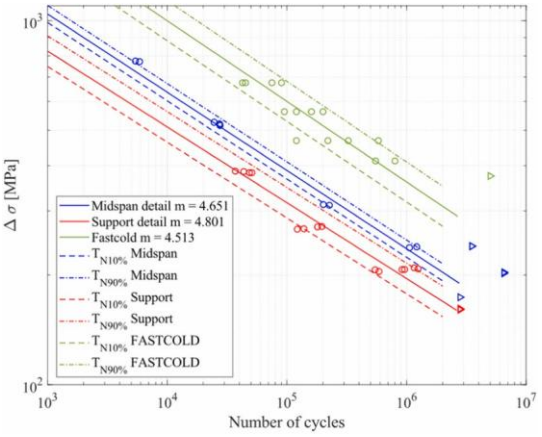

Fig. 21. Comparison between results coming from the current research and FASTCOLD project.

First of all, it can be seen that the curve proposed in FASTCOLD project (in green), is much higher than the one obtained in the framework of the presented research. This could be justified by the computation method of the stress ranges used in both approaches. Indeed, in FASTCOLD project, the

Published in : Engineering (2025), vol. 337, pp. 1–14
DOI: 10. 1016/j.engstruct.2025.120502
Status : Postprint (Author's version)

hot spot method using results from numerical simulation was applied, while in the current study, the structural hot spot method using the stresses experimentally obtained is used. Furthermore, comparing slopes of the obtained lines and the one proposed by the code, the current study (m = 4.651 for mid-span and m = 4.801 for support) gives a closest value to the one proposed by prEN1993–1–9 (m = 5), than FASTCOLD (m = 4.513). In addition, the standard deviations are smaller with $\tilde{s}_{\log N,corr,mid}$ = 0.0855 and

$\tilde{S}_{logN_{corr,support}}$ = 0.1572 for the mid-span detail and the support one respectively, than the ones obtained in FASTCOLD where

$\tilde{S}_{logN_{corr,FastCold}}$ = 0.1936. Moreover, the crack pattern is identical between the two experimental campaigns. Finally, the recommendation for the design of a Z-rail member between the two projects is consistent, as FASTCOLD is referring to a slope m = 5, using the stress range obtained by the hot spot method.

6. Conclusions

This research studied experimentally the fatigue behaviour of cold formed thin-walled rolling Z members with unequal flanges subjected to cyclic point loading on their larger lower flange. This loading configuration is usually found in rack structures where shuttles carrying pallets are circulating on such structural members used as rails. In a first step, static tests have been performed in order to assess the behaviour of the members in those specific configurations. In a second step, the fatigue life of two details was experimentally investigated (i) at mid-span of the member and (ii) at support.

The main outcomes of this study can be summarized as follows:

- A consequent fatigue campaign was conducted in which 34 elements were tested, studying two different details, with a range of force intensity included between ΔP = 3.33 kN and ΔP = 14.81 kN resulting to a number of cycles that is included between 5,416 and 6,500,000;
- For both studied details, the fatigue crack is initiating at the level of the load application, in the inside radius of the corner between the web and the lower flange on which the load is applied; then the crack penetrates through the thickness to the outer radius and develops towards the extremities of the beam;
- The obtained crack pattern demonstrates that the failure appears due to the opening of the flange compared to the web of the section, independently of the test configuration;
- The stress associated to the strains recorded by the strain gauges highlighted that a redistribution of stresses occurs in the section, as the crack is developing;
- Comparing both investigated details, the obtained S-N curves are quite similar, especially when the applied load range is considered instead of the stress range;

Published in : Engineering (2025), vol. 337, pp. 1–14
DOI: 10. 1016/j.engstruct.2025.120502
Status : Postprint (Author's version)

- The slope of the experimental fatigue curves is similar to the one proposed by prEN1993–1–9;
- Both details could be designed against fatigue using the proposed fatigue midspan curve (Fig. 14) and by computing the stresses according to Eq. 1, knowing the applied load by the wheel;
- The experimental results are in line with the ones found in the literature.

Nevertheless, it should be mentioned that this study has some limitations: only one type of section made of one steel grade was studied, the load is transferred by a wheel coming from a shuttle used by the industrial partners of the project and the horizontal position of the wheel compared to the web is constant. In addition, the whole experimental campaign was performed without longitudinal displacement of the wheel and without considering the acceleration and deceleration of the shuttle. Compared to rack storage structures, the boundary conditions have been idealised for scientific purposes in order to better manage the behaviour of the member during the experimental tests. Finally, numerical simulations validated with the test results and extending the experimental results with parametric numerical studies are under development.

This research takes place in the framework of the Walloon Region project with the acronym ACTIONS studying the behaviour of rack structures. Relevant outcomes of this project can be found in [36], [37] and [38]. The next step within this project will be to develop advanced numerical models using Abaqus software in order to predict the stresses at the level of the studied detail, with the final objective of proposing an hot spot stress design approach for this detail.

Credit authorship contribution statement

Demonceau Jean-François: Writing – review & editing, Supervision, Methodology, Conceptualization. **Bezas Marios-Zois:** Writing – review & editing. **Vermeylen Maxime:** Writing – original draft, Methodology, Investigation. **Morch Hel´ ene:** ` Writing – review & editing. **Ginckels Koenraad:** Writing – review & editing, Project administration.

Declaration of competing interest

The authors declare that they have no known competing financial interests or personal relationships that could have appeared to influence the work reported in this paper.

Acknowledgment

The authors of this publication acknowledge the Logistics in Wallonia ASBL, the Walloon Region and the Pôle MecaTech for their support in the framework of the project n°8528 entitled ACTIONS "Advanced Eurocodes Compliant Tools for Industrial Optimized Innovative Structures". The partners of the project are STOW Group, CRM and GDTech companies, as well as the university of Liège.

Data Availability

The authors do not have permission to share data.

References

[1] EN 1993-1-9: Design of steel structures - Part 1-9: Fatigue, Brussels, Comité Européen de Normalisation (CEN); 2005.

[2] prEN 1993-1-9: Design of steel structures - Part 1-9: Fatigue, Brussels, Comité Européen de Normalisation (CEN); 2023.

[3] EN15512: Systèmes de stockage en acier – Systèmes de rayonnages à palettes réglables – Principe applicable au calcul des structures, Brussels, Comité Européen de Normalisation (CEN); 2020.

[4] Majeed T., Assessment of the remaining fatigue life of a riveted steel railway bridge accounting for the mean stress [Paper presentation], ICSAS 2024, Rio de Janeiro, Brazil; 2024, June 5-8.

[5] Skoglund O, Leander J. A numerical evaluation of new structural details for an improved fatigue strength of steel bridges. Int J Fatigue 2022;160:106866. https:// doi.org/10.1016/j.ijfatigue.2022.106866.

[6] Mouradian K., Statistical evaluation of fatigue test results of butt-weld connections with imperfections [Paper presentation], NORDIC STEEL 2024, Lulea, Sweden; 2024, June 26-28.

[7] Bartsch H, Feldmann M. Revision of fatigue detail categories of plain members and mechanically fastened joints according to EC3-1-9. J Constr Steel Res 2021;179: 106549. https://doi.org/10.1016/j.jcsr.2021.106549.

[8] Christoforidou A, Baskar A, Barelts E, Kavoura F, Pavlovic M. Fatigue performance of preloaded bolted connection with oversized holes. Ce/Pap 2023;6(3–4): 1287–92. https://doi.org/10.1002/cepa.2447.

[9] Winkler M, Dürr A, Herion S, Ladendorf P. Fatigue tests on connections of hollow sections made of high-strength steel with shape-optimized gusset plates. Ce/Pap 2023;6(3–4):2429–34. https://doi.org/10.1002/cepa.2309.

[10] Misiek, T., S-N curve for screw fastenings of trapezoidal steel sheeting [Paper presentation], NORDIC STEEL 2024, Lulea, Sweden; 2024, June 26-28.

[11] Li X, Lin H, Zhao A, Wang R, Feng Z, Zhang S, Wu B, Wu C, Xu X. Experimental study on fatigue performance of double welded orthotropic steel bridge deck. J Constr Steel Res 2024;213:108418. https://doi.org/10.1016/j.jcsr.2023.108418.

[12] Ferraz G, Karabulut B, Rossi B. Fatigue resistance and reliability assessment of hot dip galvanised plates with welded transversal stiffeners. Eng Fail Anal 2024: 108577. https://doi.org/10.1016/j.engfailanal.2024.108577.

[13] Bartsch H, Drebenstedt K, Seyfried B, Feldmann M, Kuhlmann U, Ummenhofer T. Analysis of fatigue test data to reassess EN 1993-1-9 detail categories. Steel Constr 2020;13(4):280–93. https://doi.org/10.1002/stco.202000019.

[14] Bartsch H, Feldmann M. Report. Rev Detail Categ Lattice girder node Jt EC 3 2021. https://doi.org/10.2749/christchurch.2021.0428.

[15] Bartsch H, Drebenstedt K, Seyfried B, Feldmann M, Kuhlmann U, Ummenhofer T. Analysis of fatigue test data to reassess EN 1993-1-9 detail categories. Steel Constr 2020;13(4):280–93. https://doi.org/10.1002/stco.202000019.

[16] Saufnay L, Jaspart J, Demonceau J. Economic benefit of high strength steel sections for steel structures. Ce/Pap 2021;4(2–4):1543–50. https://doi.org/10.1002/ cepa.1454.

[17] Saufnay L, Demonceau J. Establishment of reliable relative price predictions for high-strength steel members. Steel Constr 2023. https://doi.org/10.1002/ stco.202300013.

[18] Saufnay L, Demonceau J. Economic and environmental assessment of high-strength steel grades. Ce/Pap 2023;6(3–4):527–32. https://doi.org/10.1002/cepa.2291.

[19] De Jesus AM, Matos R, Fontoura BF, Rebelo C, Da Silva LS, Veljkovic M. A comparison of the fatigue behaviour between S355 and S690 steel grades. J Constr Steel Res 2012;79:140–50. https://doi.org/10.1016/j.jcsr.2012.07.021.

[20] Chen H., Grondin G.Y., Driver R.G. Fatigue resistance of high-performance steel. Structural engineering report no 258. Canada: University of Alberta; 2005.

[21] Wang P, Zhang P, Wang B, Zhu Y, Xu Z, Zhang Z. Fatigue cracking criterion of high- strength steels induced by inclusions under high-cycle fatigue. J Mater Sci Technol 2023;154:114–28. https://doi.org/10.1016/j.jmst.2023.02.006.

[22] Furuya Y, Matsuoka S, Abe T, Yamaguchi K. Scr Mater 2002;46:157–62.

[23] Doubek P, Kozakov´ a K, Kunz L, Seitl S. Fatigue life of S960 high strength steel with ´ laser cladded functional surface layers. Eng Fail Anal 2024;164. https://doi.org/ 10.1016/j.engfailanal.2024.108629.

[24] Souto C, Gomes V, Figueiredo M, Correia J, Lesiuk G, Fernandes A, De Jesus A. Fatigue behaviour of thin-walled cold roll-formed steel sections. Int J Fatigue 2021; 149:106299. https://doi.org/10.1016/j.ijfatigue.2021.106299.

[25] FASTCOLD, Fatigue strength of cold-formed structural steel details. Research Program of the Research Fund for Coal and Steel, Grant Agreement Number 745982.

[26] Paralikas J, Salonitis K, Chryssolouris G. Investigation of the effects of main roll- forming process parameters on quality for a V-section profile from AHSS. Int J Adv Manuf Technol 2009;44(3–4):223–37. https://doi.org/10.1007/s00170-008-1822- 9.

[27] EN ISO 377: Steel and steel products – Location and preparation of samples and test pieces for mechanical testing, European committee for standardization, Brussels, Belgium; 1997.

[28] prEN 1993-1-3: Design of steel structures - Part 1-3: General rules – Supplementary rules for cold-formed members and sheeting, European committee for standardization, Brussels, Belgium; 2020.

[29] Union Internationale des Chemins de fer, UIC 435-2 – Palettes en bois de type Europe (EUR), UIC; 2005.

[30] Masendorf R, Müller C. Execution and evaluation of cyclic tests at constant load amplitudes–DIN50100:2016. MaterialsTesting 2018;60(10):961–8. https://doi. org/10.3139/120.111238.

[31] Schijve J. Fatigue of Structures and Material. Second ed. Springer Netherlands; 2009. https://doi.org/10.1007/978-1-4020-6808-9.

[32] Baptista C, Reis A, Nussbaumer A. Probabilistic S-N curves for constant and variable amplitude. Int J Fatigue 2017;101:312–27. https://doi.org/10.1016/j. ijfatigue.2017.01.022.

[33] Tong L, Yu Q, Zhao XL. Experimental study on fatigue behavior of butt-welded thin-walled steel plates strengthened using CFRP sheets. Thin-Walled Struct 2020; 147. https://doi.org/10.1016/j.tws.2019.106471.

[34] Kovesdi B, Dunai L. Fatigue life of girders with trapezoidally corrugated webs: an ¨ experimental study. Int J Fatigue 2014;64:22–32. https://doi.org/10.1016/j. ijfatigue.2014.02.017.

[35] DIN50100: Load controlled fatigue testing – Execution and evaluation of cyclic tests at constant load amplitudes on metallic specimens and components (in German), Beuth, Berlin, Germany; 2016.

[36] Vermeylen M, Bezas M, Crispin M, Jaspart J, Demonceau J. Lateral-torsional buckling of beams made of mono-symmetrical thin-walled sections. Ce/Pap 2023;6 (3–4):1649–54. https://doi.org/10.1002/cepa.2358.

[37] Vermeylen M., Bezas M., Morch H., Ginckels K., Demonceau J., Bolted connection between thin-walled and thick elements made of cold-formed section [Paper presentation], ICSAS 2024, Rio de Janeiro, Brazil; 2024, June 5-8.

[38] Bezas M-Z, Vermeylen M, Morch H, Ginckels K, Demonceau J-F. Design guidelines for SHS thin-walled columns with large holes at their extremities. Steel Constr 2024. https://doi.org/10.1002/stco.202400024.